

# Analytic Model of Radial Sensitivity in Cylindrical PET Systems Based on First Principles

Boheng Lin, Zizhuo Xie, Bo Zhang, Lin Wan, Ao Qiu, Qingguo Xie

**Abstract**—In cylindrical positron emission tomography (PET) systems, the center of the field of view (CFOV) is commonly treated as the point of maximum system sensitivity. This is reflected in standardized protocols such as NEMA NU 2-2018, which prescribe measurements at the center of the field of view (FOV), and system evaluation reports that adhere to this standard. Existing experimental studies report varying sensitivity patterns across the radial plane, with some suggesting comparable or higher sensitivity at off-center positions and others documenting more complex, non-monotonic trends. Despite the existence of these discrepancies, a theoretical description of the expected sensitivity distribution across the radial plane, derived from first principles, has not been clearly established. In this work, we derive an analytic model of the radial-plane sensitivity distribution for a cylindrical PET system, based solely on idealized scanner geometry and detection physics. To our knowledge, this is the first closed-form theoretical formulation of its kind, providing a fundamental description of sensitivity variation in the radial plane under ideal conditions. The model excludes system-specific effects such as detector efficiency and crystal geometry, and therefore establishes a generalizable baseline that can inform both conceptual understanding and practical analysis. To assess the applicability of the model in real-world systems, we perform Monte Carlo simulations and physical experiments on a representative PET system. The measured and simulated sensitivity distributions show good agreement with the theoretical predictions, with some key deviations attributable to implementation-specific factors. In addition to serving as a reference for interpreting inconsistencies in empirical measurements, this work contributes foundational knowledge that may inform future system design, quantitative analysis, and textbook-level descriptions of PET system behavior.

**Index Terms**—radial sensitivity, sensitivity distribution, positron emission tomography, cylindrical PET, field-of-view, signal-to-noise ratio

## I. INTRODUCTION

Positron Emission Tomography (PET) is widely used for diagnosing and monitoring cancer, neurological disorders, and cardiovascular conditions [1]–[4]. Among the many factors

This work did not involve human subjects or animals in its research.

All authors declare that they have no known conflicts of interest in terms of competing financial interests or personal relationships that could have an influence or are relevant to the work reported in this paper.

This work was partially supported by the National Natural Science Foundation of China (NSFC) under grant No. 62250002, 62050288, and 61927801.

Boheng Lin and Lin Wan are with the School of Software Engineering, Huazhong University of Science and Technology, Wuhan, 430074 China.

Zizhuo Xie is with Eleanor Roosevelt College, University of California San Diego, La Jolla, CA 92093 USA.

Bo Zhang, Ao Qiu, and Qingguo Xie are with the Department of Biomedical Engineering, Huazhong University of Science and Technology, Wuhan, 430074 China.

Correspondence should be addressed to Zizhuo Xie (samxieacademics@gmail.com), Qingguo Xie (qgxie@hust.edu.cn), and Bo Zhang (bozhang-pet@hust.edu.cn).

influencing PET performance, sensitivity is one of the most critical metrics [5]–[7].

Standardized protocols such as NEMA NU 2-2018 [8] define sensitivity measurement procedures at the center of the field of view (CFOV) and at a radial offset of 10 cm. This convention, used in many system performance studies [9]–[12], implicitly assumes that sensitivity is either maximized or sufficiently characterized near the CFOV.

However, empirical studies present inconsistent findings. Some report higher sensitivity at 10 cm than at the CFOV [10], [12], others report the opposite [9], and a few describe non-monotonic trends across the radial plane [13].

Empirical inconsistencies in reported radial sensitivity trends underscore the absence of a theoretical baseline. To date, the sensitivity distribution with respect to radial position has not been derived from first principles. Although some prior studies have proposed mathematical formulations for sensitivity at the CFOV [11], a general theoretical model describing how sensitivity varies across the entire radial plane has not been established.

In this work, we present a closed-form analytic model of the radial-plane sensitivity distribution for an idealized cylindrical PET scanner. The model is derived from geometric principles and simplified detection physics. Implementation-specific considerations, while important for full system performance, are beyond the scope of this study and will be addressed in future work. Beyond its theoretical value, the model can serve as a baseline for interpreting empirical sensitivity measurements and may inform in future system design and analysis.

The remainder of this paper is organized as follows. Section II presents the theoretical analysis, including the geometric modeling of the cylindrical PET system and the derivation of the closed-form sensitivity function under idealized conditions. Section III describes the Monte Carlo simulations and physical experiments conducted to assess the applicability of the theoretical model. Section IV compares the theoretical predictions with the empirical results, highlighting areas of agreement and deviation. Finally, Section V concludes the paper with a summary of the contributions.

### A. Problem Definition

This study quantitatively characterizes the relationship between system sensitivity in a cylindrical PET scanner and the spatial position of a radiation source in the radial plane, using a distribution function  $S_g$  to describe sensitivity as a function of radial position.

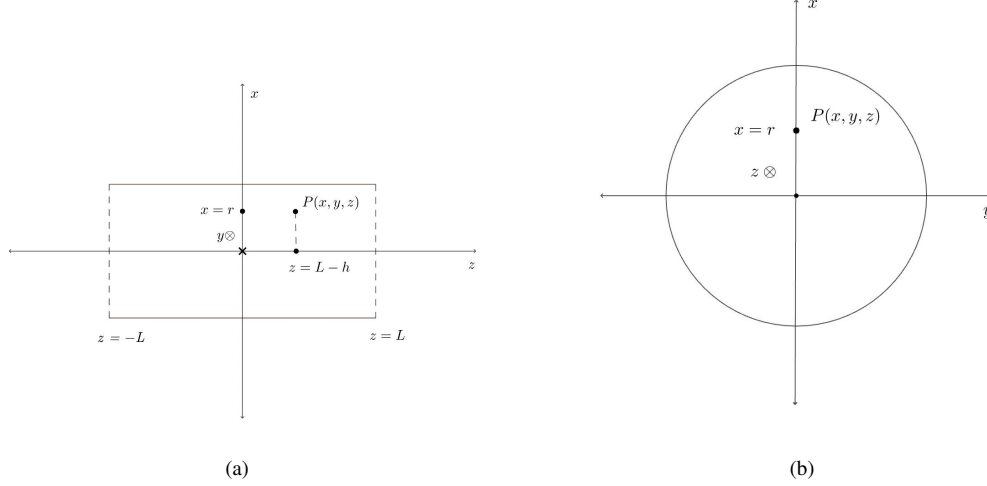


Fig. 1. Diagrams showing the PET cylindrical system within the defined spatial framework: (a) view sliced along the axial direction, and (b) view sliced along the trans-axial direction

### B. Geometric Modeling

We define the system within the following spatial framework:

- Define the origin as  $(0, 0, 0)$ .
- Define the  $Z$ -axis as the horizontal axis.
- Define the  $X$ -axis as the vertical axis.
- Define the  $Y$ -axis perpendicular to both the  $Z$ -axis and the  $X$ -axis, completing a right-handed coordinate system.

The cylindrical PET system is oriented so that:

- Its axial direction aligns with the  $Z$ -axis.
- Its cross-sectional planes are parallel to the  $XY$ -plane, representing slices of the cylinder.
- The cylinder extends from  $z = -L'$  to  $z = L'$  along the  $Z$ -axis, and it has a constant radius  $R'$  in the  $XY$ -plane. It can be represented by the equation:

$$x^2 + y^2 = R'^2, \quad -L' \leq z \leq L'. \quad (1)$$

The spatial position of the radiation source is represented by a point  $P(r', y', L' - h')$ , where:

- $r'$  and  $y'$  specify the source's position within the  $XY$ -plane (cylindrical cross-section).
- $L' - h'$  specifies the source's position along the axial  $Z$ -axis, where  $h'$  is the  $Z$ -axis distance between  $z = L'$  and the  $z$ -coordinate of point  $P$ .

Since  $L'$ ,  $R'$ ,  $r'$ , and  $h'$  are chosen arbitrarily, we can normalize to simplify later operations. Let:  $R = R'/R' = 1$ ,  $L = L'/R'$ ,  $r = r'/R'$ ,  $h = h'/R'$ . The cylinder can now be represented as:

$$x^2 + y^2 = 1^2, \quad -L \leq z \leq L. \quad (2)$$

And the point  $P$  is now  $P(r, y, L - h)$ .

This has been visually summarized in Figure 1.

### C. Definition of Sensitivity

The sensitivity of a cylindrical PET scanner is defined as the ratio of recorded true coincidence events to the radioactivity

of the positron-emitting source [7], [8], [14]–[16]. Geometric sensitivity is governed by the solid angle subtended by the detector walls when viewed from the position of the radiation source [17], [18]. Specifically, the ratio of recorded true coincidence events to the source's radioactivity can be expressed in terms of the fraction of the total solid angle of the space subtended by the detector walls; let the geometric sensitivity determined by the solid angle be  $S_g$ :

$$S_g := \frac{\text{solid angle subtended by detector walls}}{4\pi} \quad (3)$$

For a positron-electron annihilation event to be classified as a true coincidence, both of the resulting 511 keV gamma photons must be detected by opposing detector modules on the PET scanner ring within a defined coincidence time window, thereby defining a valid line of response (LOR) along which the annihilation is assumed to have occurred [14], [19]. In a cylindrical PET system, the axial extremities of the scanner are open circular regions, hereafter referred to as Cap 1 and Cap 2. A positron-electron annihilation event is classified as a true coincidence if and only if both resulting 511 keV gamma photons are retained within the detection volume—that is, neither photon exits the system through Cap 1 or Cap 2.

The probability of a gamma photon escaping through one of the caps before interacting with the detector walls is determined by the solid angle subtended by the caps at the position of the radiation source [20]. Denote this solid angle as  $\Omega$ . Then the geometric sensitivity for coincidence events in a cylindrical PET system can be expressed as:

$$S_g = (4\pi - \Omega)/4\pi = 1 - \Omega/4\pi. \quad (4)$$

### D. Computing Solid Angle

The computation of  $S_g$  reduces to determining  $\Omega$ , which is obtained by integrating the differential solid angle over the area of the caps. The differential solid angle is given by:

$$d\Omega = \cos(\theta) dA/\rho^2, \quad (5)$$

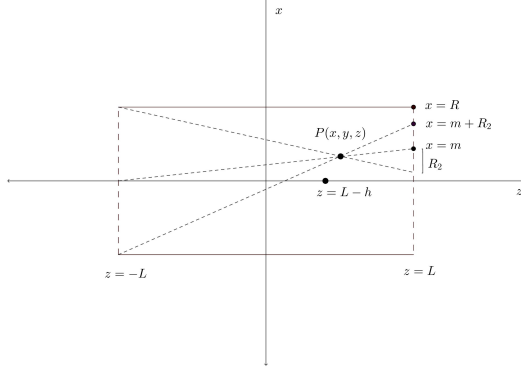


Fig. 2. Diagram showing the projection of Cap 2 (left cap) onto Cap 1 (right cap) through the point  $P$ , to form Cap  $2'$

where  $dA$  is the infinitesimal surface area element of on the caps,  $\theta$  is the angle between the vector connecting the source point  $P$  to  $dA$  and the surface normal, and  $\rho$  is the distance between  $P$  and  $dA$ . Substituting  $\cos(\theta) = h/\rho$ , where  $h$  is the perpendicular distance from  $P$  to  $dA$ , we can rewrite  $d\Omega$  as:

$$d\Omega = h dA / \rho^3. \quad (6)$$

Since the system exhibits reflectional symmetry about the XY-plane, it is sufficient to analyze only the right half of the geometry. Without loss of generality, we therefore restrict attention to the region bounded by:  $x^2 + y^2 \leq R^2$ ,  $0 \leq z \leq L$ . To account for the omitted left half, the left end cap (Cap 2) is projected onto the plane of the right end cap (Cap 1) located at  $z = L$ , resulting in the projected cap, denoted as Cap  $2'$ , as illustrated in Figure 2.

The projected Cap  $2'$  will have radius  $R_2$ :  $R_2 = h/(2L-h)$ . The center of Cap  $2'$  will be a distance  $m$  from the center of Cap 1, where:  $m = r \cdot 2L/(2L-h)$ . The total solid angle  $\Omega$  is the union of the solid angles subtended by Cap 1 ( $\Omega_1$ ) and Cap  $2'$  ( $\Omega'_2$ ):  $\Omega = \Omega_1 \cup \Omega'_2$ .

Furthermore, due to the circular symmetry of the system within the XY-plane, it is sufficient to consider radial offsets along the x-axis only. This allows us to disregard the y-coordinate and simplify the source position to the point  $P(r, 0, L-h)$ .

Now, consider the integration of  $d\Omega$ . The distance  $\rho$  from a point  $(x, y, L)$  on the plane  $z = L$  in the system to  $P$  is given by:  $\rho = [(x-r)^2 + y^2 + h^2]^{1/2}$ . To find  $\Omega$ , we integrate  $d\Omega$  over the total area of interest, call it  $H$ :

$$\Omega = \iint_H \frac{h dA}{\rho^3} = \iint_H \frac{h dy dx}{[(x-r)^2 + y^2 + h^2]^{3/2}} \quad (7)$$

We can turn this integral over an area into a line integral over the boundaries of the area by using Green's Theorem [21] and the fact that:

$$\int \frac{dx}{(x^2 + k^2)^{3/2}} = \frac{x}{k^2 \cdot \sqrt{x^2 + k^2}} + C \quad (8)$$

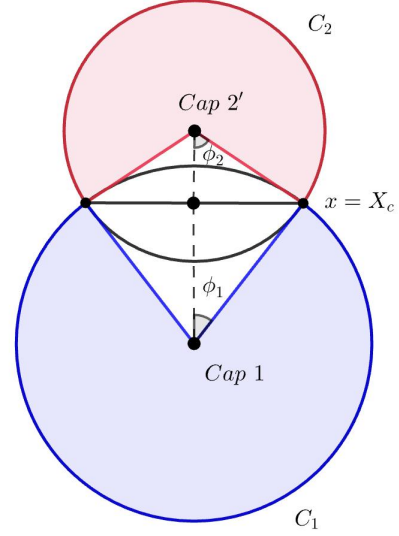


Fig. 3. Diagram displaying the case when Cap 1 and Cap  $2'$  overlap. The blue arc of Cap 1 is denoted as  $C_1$  and the red arc of Cap  $2'$  is denoted as  $C_2$

Substituting the integral variable of the above formula into  $y$ , taking  $C = 0$ , and applying Green's Formula, we have:

$$\begin{aligned} \Omega &= \iint_H \frac{-h dy dx}{[(x-r)^2 + y^2 + h^2]^{3/2}} \\ &= \oint_{\partial H} \frac{-h y dx}{[(x-r)^2 + h^2] \cdot [(x-r)^2 + y^2 + h^2]^{1/2}} \end{aligned} \quad (9)$$

Finally, the geometric sensitivity  $S_g$  can be expressed as:

$$S_g = 1 - \Omega/2\pi. \quad (10)$$

## II. THEORETICAL ANALYSIS AND DERIVATION

### A. Case Analysis

Consider the union of Cap 1 and Cap  $2'$ . This can be split into two cases:

- 1) When Cap  $2'$  is fully enclosed in Cap 1, i.e.  $m+R_2 \leq R$ , the union is simply Cap 1.
- 2) When Cap  $2'$  extends beyond the boundary of Cap 1, i.e.  $m+R_2 > R$ , the union consists of the entirety of Cap 1 plus the protruded area of Cap  $2'$ .

1) *Case 1:* In this case, Cap  $2' \subseteq$  Cap 1,  $\partial H = x^2 + y^2 = R^2$ . We can facilitate the integral by transforming  $\partial H$  into parametric form.

Take  $\theta \in [0, 2\pi)$ ,  $x = \cos(\theta)$ ,  $y = \sin(\theta)$ , then

$$\Omega = \int_0^{2\pi} \frac{h}{[(\cos \theta - r)^2 + \sin^2 \theta + h^2]^{1/2}} \cdot \frac{\sin^2 \theta d\theta}{(\cos \theta - r)^2 + h^2} \quad (11)$$

$$S_g = 1 - \frac{1}{2\pi} \int_0^{2\pi} \frac{h}{[(\cos \theta - r)^2 + \sin^2 \theta + h^2]^{1/2}} \cdot \frac{\sin^2 \theta d\theta}{(\cos \theta - r)^2 + h^2} \quad (12)$$

2) *Case 2*: In this case, Cap 2' overlaps with Cap 1, thus we integrate over the contour of the protruded area in addition to the contour of Cap 2' that is not within Cap 1. To do this, we must determine the two points of intersection between Cap 1 and Cap 2'.

The X-coordinate, denoted by  $X_c$ , of the common chord of two intersecting circles is giving by:

$$X_c = (1 - R_2^2 + m^2)/2m \quad (13)$$

With  $X_c$ , we can determine the central angles,  $\phi_1$  and  $\phi_2$ , of both caps for the intersection. For Cap 1,  $\cos(\phi_1) = X/R$ , where  $\phi_1$  is half the central angle for Cap 1. For Cap 2',  $\cos(\phi_2) = (m - X)/R_2$ , where  $\phi_2$  is half the central angle for Cap 2'.

Define the arc of Cap 1 as  $C_1$  and the arc of Cap 2' as  $C_2$ , as illustrated by Figure 3, then  $\partial H = C_1 + C_2$ , and the integral becomes:

$$\begin{aligned} \Omega &= \int_{C_1} \frac{-hydx}{[(x-r)^2 + h^2] \cdot [(x-r)^2 + y^2 + h^2]^{1/2}} \\ &+ \int_{C_2} \frac{-hydx}{[(x-r)^2 + h^2] \cdot [(x-r)^2 + y^2 + h^2]^{1/2}} \\ &= \int_{\phi_1}^{2\pi-\phi_1} \frac{h}{[(\cos\theta - r)^2 + \sin^2\theta + h^2]^{1/2}} \\ &\quad \cdot \frac{\sin^2\theta d\theta}{(\cos\theta - r)^2 + h^2} \\ &+ \int_{-\pi+\phi_2}^{\pi-\phi_2} \frac{h}{[(R_2\cos\theta + m - r)^2 + R_2^2\sin^2\theta + h^2]^{1/2}} \\ &\quad \cdot \frac{R_2^2\sin^2\theta d\theta}{(R_2\cos\theta + m - r)^2 + h^2} \end{aligned} \quad (14)$$

$$\begin{aligned} S_g &= 1 - \frac{\Omega}{2\pi} \\ &= 1 - \frac{1}{2\pi} \left( \int_{\phi_1}^{2\pi-\phi_1} \frac{h}{[(\cos\theta - r)^2 + \sin^2\theta + h^2]^{1/2}} \right. \\ &\quad \cdot \frac{\sin^2\theta d\theta}{(\cos\theta - r)^2 + h^2} \\ &\quad \left. + \int_{-\pi+\phi_2}^{\pi-\phi_2} \frac{h}{[(R_2\cos\theta + m - r)^2 + R_2^2\sin^2\theta + h^2]^{1/2}} \right. \\ &\quad \cdot \left. \frac{R_2^2\sin^2\theta d\theta}{(R_2\cos\theta + m - r)^2 + h^2} \right) \end{aligned} \quad (15)$$

### B. Theoretical Result

We consolidate the two cases into a single result, where the general geometric sensitivity of the system is modeled by the following distribution:

$$S_g = \begin{cases} \text{equation (12),} & m + R_2 \leq R \\ \text{equation (15),} & m + R_2 > R \end{cases} \quad (16)$$

Using MATLAB [22], we plot the sensitivity  $S_g$  based on equation (16) with 100 evenly spaced points in the range  $[0, R]$ . The dimensions of the PET system were set to  $R = 405$

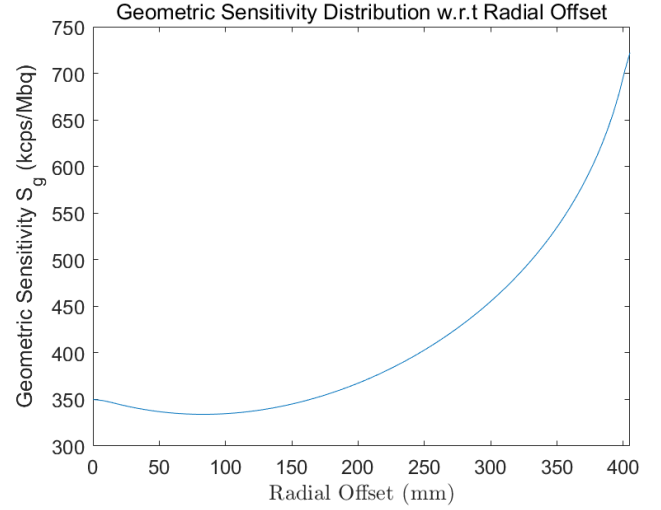


Fig. 4. Plot of the geometric sensitivity as a function of radial offset, calculated based on equation (16). The plot considers 100 evenly spaced points within  $[0, R]$  for a PET system with dimensions  $R = 405$  mm and  $L = 153$  mm

mm and  $L = 153$  mm. The resulting plot is shown in Figure 4.

## III. EXPERIMENTS AND SIMULATIONS

### A. GATE Simulations

Simulations were performed in GATE [23] using a PET scanner with a radius  $R = 403.8$  mm and an axial length  $2L = 306$  mm. The scanner used lutetium yttrium osmium (LYSO) scintillator crystals, arranged in a  $6 \times 6$  grid within each detector block. Each crystal had dimensions of  $20.0$  mm  $\times$   $3.9$  mm  $\times$   $3.9$  mm.

The system consists of three detector rings, each ring containing 48 detector modules, totaling 144 modules. Each detector module contains  $1 \times 2 \times 4$  sub-blocks, with dimensions  $20.0$  mm  $\times$   $25.5$  mm  $\times$   $25.5$  mm.

A cylindrical  $^{18}\text{F}$  radioactive source with a radius of  $0.01$  mm and a length of  $700$  mm was used. The source had an activity of  $7.4$  MBq ( $7.4 \times 10^6$  Bq).

The following thresholding methods were applied:

- **Energy Window Filtering:** Only events with energy levels within the window of  $[420, 650]$  keV were considered valid.
- **Time Window Filtering:** Only photon pairs that were detected within  $4$  ns of each other were considered true coincidence events.
- **Distance Thresholding/FOV:** Events detected outside the FOV radius were discarded. Simulations were conducted for  $250$  mm FOV radius and  $300$  mm FOV radius.

Sensitivity values were obtained at radial offsets in increments of  $25$  mm, covering a range from  $0$  mm to  $400$  mm, and at axial slices in increments of  $25$  mm, covering a range from  $0$  mm to  $75$  mm [24]. These values were calculated in accordance with the NEMA standard [8]. The corresponding plots are shown in Figure 5.

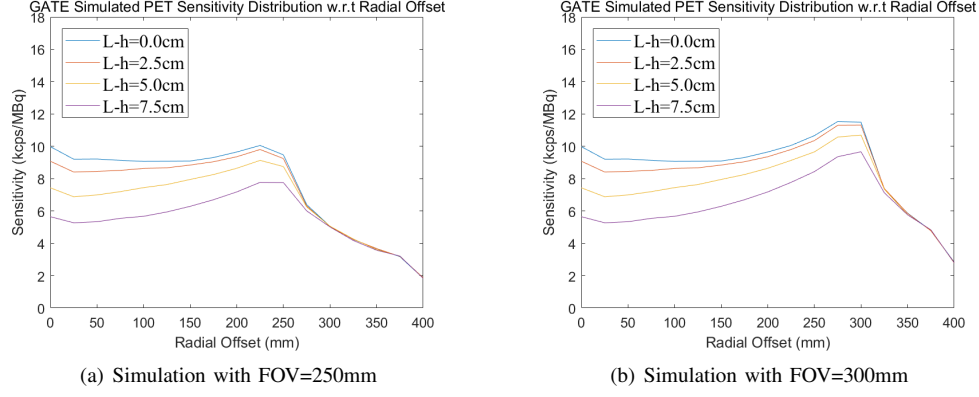


Fig. 5. Distributions for a) sensitivity w.r.t radial offset for a FOV radius of 250 mm across 4 axial slices, and b) sensitivity w.r.t radial offset for a FOV radius of 300 mm across 4 axial slices

### B. Experiments

Experiments were performed using the same PET scanner dimensions as in the simulations, with a ring radius of 403.8 mm and an axial length of 306 mm.

A cylindrical  $^{18}\text{F}$  radioactive source with a radius of 0.01 mm and a length of 700 mm was used, with an activity of 7.4 MBq. Data collection and sensitivity calculations followed the NEMA standard [8], ensuring comparability with established benchmarks.

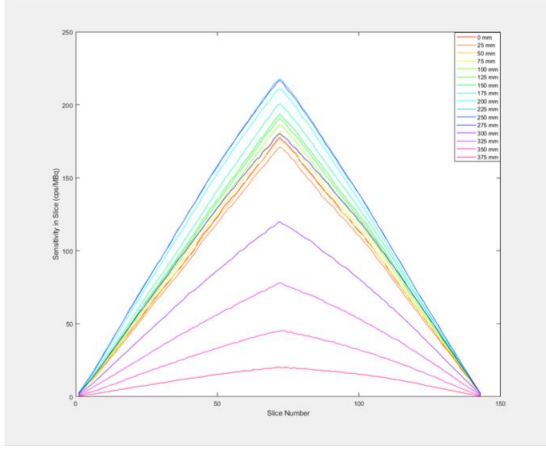


Fig. 6. Experimental sensitivity across axial slices for 16 different radial offsets

The following thresholding methods were applied:

- **Energy Window Filtering:** Only events with energy levels within the window of [420, 650] keV were considered valid.
- **Time Window Filtering:** Only photon pairs detected within 4 ns of each other were considered true coincidence events.
- **Distance Thresholding/FOV:** A 250 mm FOV radius was enforced, discarding events detected beyond this range.

Sensitivity values were measured after subtraction of random coincidences. Figure 6 presents the sensitivity distribution across 150 axial slices at 16 radial offsets ranging from 0 mm to 375 mm [24]. Figure 7 illustrates the sensitivity distribution

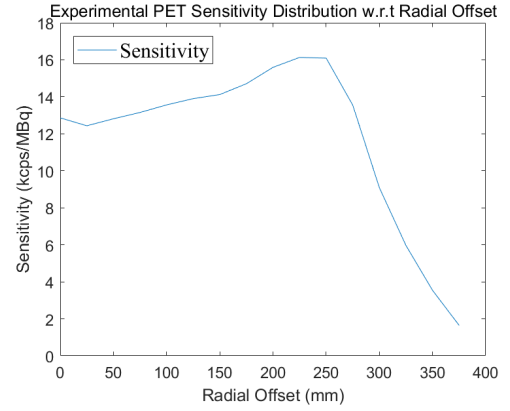


Fig. 7. Experimental sensitivity w.r.t radial offset. The sensitivity measurements were taken at 25 mm intervals from 0 mm to 375 mm, resulting in 16 distinct points plotted in the figure

with respect to radial offset at the center slice of the PET scanner.

### IV. DISCUSSION

The theoretical model derived in this study predicts that system sensitivity in a cylindrical PET scanner first slightly decreases then increases with radial offset and reaches a maximum near the periphery of the FOV. To evaluate the applicability of this model, we compared its predictions against results obtained from simulations and physical measurements. The results are put side-by-side in Figure 8.

The simulation results largely mirror the theoretical curve, confirming the expected increase in sensitivity with radial offset and locating the peak near the outer radial edge of the scanner's FOV. Empirical results, while consistent with this general trend, show noticeable differences. In particular, both the simulation and experimental sensitivity distribution exhibit a sharp drop off past a certain radial offset. These differences are to be expected, given that the experimental data reflect a range of real-world factors that are deliberately excluded from the idealized model.

Despite these deviations, the agreement between the theoretical and empirical trends at a qualitative level is both

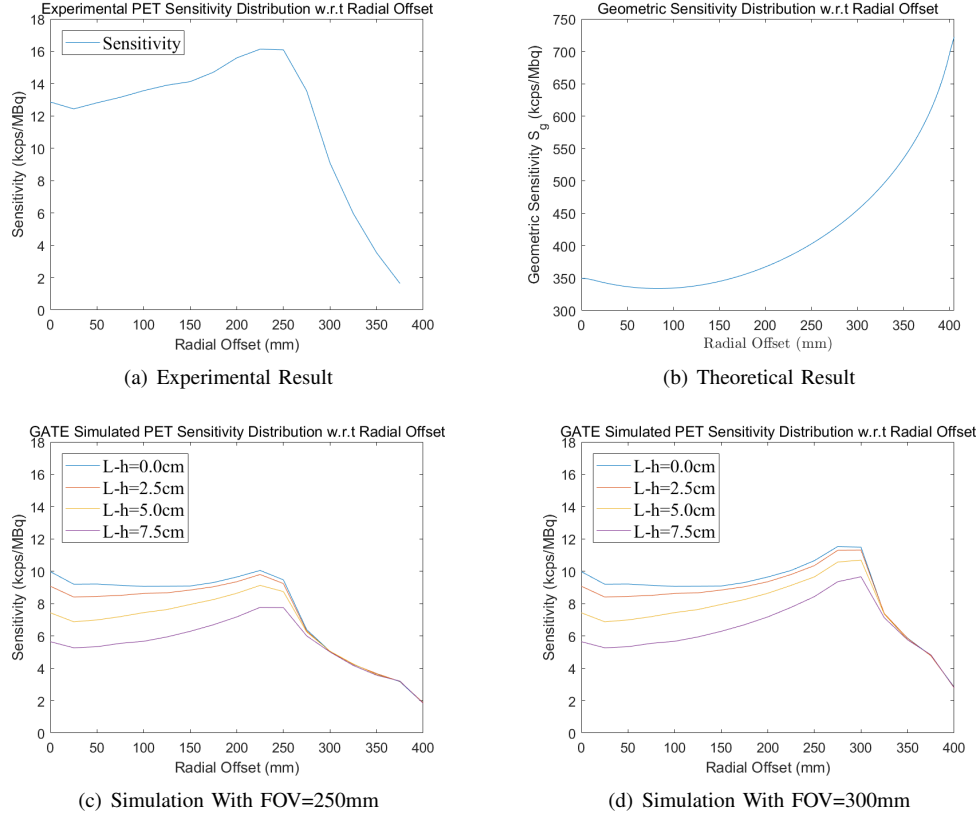


Fig. 8. Side-by-side compilation of previous diagrams of experimental, theoretical, and simulated sensitivity for direct comparison

meaningful and reassuring. The model accurately captures the overall behavior of sensitivity across the radial plane and establishes a reliable reference for identifying and interpreting departures in practical systems. The regions of agreement—especially the general increase in sensitivity away from the center—affirm the validity of the model’s prediction, while the observed differences highlight the influence of non-ideal system characteristics.

Future work will focus on investigating system-level and implementation-specific factors that influence sensitivity, to better understand their contribution to the discrepancies between theoretical predictions and empirical observations. By systematically introducing variables into extended simulations or layered analytic models, we aim to quantify their individual contributions and refine the theoretical description accordingly.

## V. CONCLUSION

The analytic model derived in this study provides a first-principles description of the radial-plane sensitivity distribution for cylindrical PET systems under idealized conditions. By isolating the system geometry and basic detection physics, the model establishes a theoretical baseline that had not previously been articulated in closed form. The formulation presented here contributes a conceptual tool for understanding how system sensitivity varies with radial position in an ideal setting.

Beyond its conceptual value, the model can also serve as a practical baseline for system evaluation, scanner calibration,

and design analysis. By excluding confounding factors such as detector efficiency, crystal geometry, attenuation, or time-of-flight corrections, the theoretical curve can be used to isolate and study the influence of these variables in real systems. Thus, this work is not intended to refute prior assumptions or findings, but rather to supplement them by providing a precise theoretical framework.

## ACKNOWLEDGMENT

The authors gratefully acknowledge the support provided by RAYSOLUTION Healthcare Co., Ltd. for this work. The authors also extend their sincere appreciation to the PET Center of Union Hospital, Tongji Medical College, Huazhong University of Science and Technology, for the generous provision of radioisotopes and related resources.

## REFERENCES

- [1] Z. Li, A. A. Gupte, A. Zhang, and D. J. Hamilton, “Pet imaging and its application in cardiovascular diseases,” *Methodist DeBakey Cardiovascular Journal*, vol. 13, no. 1, pp. 29–32, 2017.
- [2] M. D. Farwell, D. A. Pryma, and D. A. Mankoff, “Pet/ct imaging in cancer: Current applications and future directions,” *Cancer*, vol. 120, no. 22, pp. 3433–3445, 2014.
- [3] M. Politis and P. Piccini, “Positron emission tomography imaging in neurological disorders,” *Journal of Neurology*, vol. 259, pp. 1769–1780, 2012.
- [4] A. Gonzalez-Montoro, A. J. Gonzalez, S. Pourashraf, R. S. Miyaoka, P. Bruyndonckx, G. Chinn, L. A. Pierce, and C. S. Levin, “Evolution of pet detectors and event positioning algorithms using monolithic scintillation crystals,” *IEEE Transactions on Radiation and Plasma Medical Sciences*, vol. 5, no. 3, pp. 282–305, 2021.



- [5] N. C. Nguyen, J. L. Vercher-Conejero, A. Sattar, M. A. Miller, P. J. Maniawski, D. W. Jordan, R. F. M. Jr., K.-H. Su, J. K. O'Donnell, and P. F. Faulhaber, "Image quality and diagnostic performance of a digital pet prototype in patients with oncologic diseases: Initial experience and comparison with analog pet," *Journal of Nuclear Medicine*, vol. 56, no. 9, pp. 1378–1385, 2015.
- [6] E. Calderón, F. P. Schmidt, W. Lan, S. Castaneda-Vega, A. S. Brendlin, N. F. Trautwein, H. Dittmann, C. la Fougère, and L. S. Kiefer, "Image quality and quantitative pet parameters of low-dose [18f]fdg pet in a long axial field-of-view pet/ct scanner," *Diagnostics*, vol. 13, no. 20, p. 3240, 2023.
- [7] T. F. Budinger, "Pet instrumentation: What are the limits?," *Seminars in Nuclear Medicine*, vol. 28, no. 3, pp. 247–267, 1998. The Coming Age of Pet (Part 1).
- [8] National Electrical Manufacturers Association (NEMA), *NEMA Standards Publication NU 2-2018: Performance Measurements of Positron Emission Tomographs*. National Electrical Manufacturers Association, Rosslyn, VA, USA, 2018. Accessed pages 17–20 for performance measurements related to PET systems.
- [9] B. W. Jakoby, Y. Bercier, M. Conti, M. E. Casey, B. Bendriem, and D. W. Townsend, "Physical and clinical performance of the mct time-of-flight pet/ct scanner," *Physics in Medicine and Biology*, vol. 56, no. 8, pp. 2375–2389, 2011.
- [10] S. Chen, P. Hu, Y. Gu, H. Yu, and H. Shi, "Performance characteristics of the digital umi550 pet/ct system according to the nema nu2-2018 standard," *EJNMMI Physics*, vol. 7, no. 1, p. 43, 2020.
- [11] D. A. B. Bonifacio, R. Latella, H. M. Murata, J. M. Benlloch, A. J. Gonzalez, P. Lecoq, and G. Konstantinou, "Analytical study of the sensitivity of cylindrical pet systems based on bulk materials and metascintillators," *IEEE Transactions on Radiation and Plasma Medical Sciences*, 2023. Early Access.
- [12] A. Chicheportiche, R. Marciano, and M. Orevi, "Comparison of nema characterizations for discovery mi and discovery mi-dr tof pet/ct systems at different sites and with other commercial pet/ct systems," *EJNMMI Physics*, vol. 7, no. 1, p. 4, 2020.
- [13] E. P. Visser, J. A. Disselhorst, M. Brom, P. Laverman, M. Gotthardt, W. J. Oyen, and O. C. Boerman, "Spatial resolution and sensitivity of the inveon small-animal pet scanner," *Journal of Nuclear Medicine*, vol. 50, no. 1, pp. 139–147, 2009.
- [14] S. R. Cherry and M. Dahlbom, *PET: Physics, Instrumentation, and Scanners*. Unknown Publisher, Unknown Year. Comprehensive guide on the physics and instrumentation of positron emission tomography (PET).
- [15] G. Amoyal, V. Schoepff, F. Carrel, M. Michel, N. B. de Lanaute, and J. Angélique, "Development of a hybrid gamma camera based on timepix3 for nuclear industry applications," *Nuclear Instruments and Methods in Physics Research Section A: Accelerators, Spectrometers, Detectors and Associated Equipment*, vol. 987, p. 164838, 2021.
- [16] M. T. Madsen, "Advances in pet imaging," *Correspondence Continuing Education Courses for Nuclear Pharmacists and Nuclear Medicine Professionals*, vol. 10, no. 5, 2004. Accredited by the American Council on Pharmaceutical Education, Program No. 039-000-02-005-H04, 3.5 Contact Hours, 0.35 CEUs.
- [17] D. Perez-Benito, R. Chil, L. A. Hidalgo-Torres, and J. J. Vaquero, "Scintillator geometrical considerations for detectors based on hexagonal sipms," *IEEE Transactions on Radiation and Plasma Medical Sciences*, vol. 7, pp. 684–691, September 2023.
- [18] D. C. Ficke, J. T. Hood, and M. M. Ter-Pogossian, "A spheroid positron emission tomograph for brain imaging: A feasibility study," *Journal of Nuclear Medicine*, vol. 37, no. 7, pp. 1219–1225, 1996.
- [19] S. Vallabhajosula, "Radioactivity detection: Pet and spect scanners," in *Molecular Imaging and Targeted Therapy*, ch. 5, Springer, 2023.
- [20] M. L. A. Camborde, *Detection to Improve the Quality of PET Imaging*. PhD thesis, McGill University, 2001. Accessed: 2024-02-21.
- [21] M. Bourlard and S. Nicaise, "Abstract green formula and applications to boundary integral equations," *Numerical Functional Analysis and Optimization*, vol. 18, no. 7-8, pp. 667–689, 1997.
- [22] The MathWorks, Inc., "Matlab, version r2023a," <https://www.mathworks.com/products/matlab.html>, 2023. Natick, Massachusetts, The MathWorks, Inc.
- [23] S. Jan, G. Santin, D. Strul, S. Staelens, K. Assié, D. Autret, S. Avner, R. Barbier, M. Bardiès, P. M. Bloomfield, D. Brasse, V. Breton, P. Bruyndonckx, I. Buvat, A. F. Chatzioannou, Y. Choi, Y. H. Chung, C. Comtat, D. Donnarieix, L. Ferrer, S. J. Glick, C. J. Groiselle, D. Guez, P.-F. Honore, S. Kerhoas-Cavata, A. S. Kirov, V. Kohli, M. Koole, M. Krieguer, D. J. van der Laan, F. Lamare, G. Largeron, C. Lartzien, D. Lazaro, M. C. Maas, L. Maigne, F. Mayet, F. Melot, C. Merheb, E. Pennacchio, J. Perez, U. Pietrzyk, F. R. Rannou, M. Rey, D. R. Schaart, C. R. Schmidtlein, L. Simon, T. Y. Song, J.-M. Vieira, D. Visvikis, R. V. de Walle, E. Wieërs, and C. Morel, "Gate: a simulation toolkit for pet and spect," *Physics in Medicine & Biology*, vol. 49, p. 4543, sep 2004.
- [24] B. Lin, "Simulated and experimental radial sensitivity measurements for cylindrical pet systems," 2025. Available at <https://dx.doi.org/10.21227/xxqh-9478>.